28th AIAA/CEAS Aeroacoustics 2022 Conference, 14-17 June 2022, Southampton, UK.
DOI: 10.2514/6.2022-3037

Measurement and Modelling of Noise-Power-Distance Curves of a Fixed-Wing UAV

Daniel Amargianitakis * and Rod Self †
Institute of Sound and Vibration Research, University of Southampton, Southampton, Hampshire, SO17 1BJ

Anderson R. Proença‡
School of Aerospace, Transport and Manufacturing, Cranfield University, Cranfield, MK43 0AL, UK

Cameron Boyd§, Oliver Westcott¶, Mario Ferraro‖, Mehmet Ali Erbil** and Robert Entwistle††
Computational Engineering and Design Group, University of Southampton, Southampton, Hampshire, SO17 1BJ

This paper presents an investigation into the noise produced by an unmanned aerial vehicle (UAV). The platform used, 'Spotter', is a fixed-wing, light UAV comprising a 4-meter wingspan. Spotter was originally designed to perform long-endurance, all-weather patrol missions in coastal and maritime environments. This vehicle has been continuously upgraded and is now used in a broader range of applications. Increasing demand by research and industrial partners, as well as the UK Civil Certification Authority (CAA) has led to a survey of the Spotter's in-flight noise footprint. The CAA Operating Safety Case of this platform is currently being updated and the major findings are presented in the paper. Preliminary results were obtained in flight tests performed at the Draycot Aerodrome over two expeditions in the summer of 2021, in the UK. A series of flyovers, takeoff and landing operations were measured. Flyovers were performed at constant altitude at series of power settings, incrementing from low to maximum power output. These measurements are then used to generate Noise-Power-Distance curves for the Spotter UAV. Static directivity characteristics of the dual propeller setup were also measured, with intent of feeding into future airport exposure studies.

I. Nomenclature

A	=	contour area, m^2
d	=	slant distance, m
f	=	frequency, Hz
h	=	altitude, m
$L_{A,max}$	=	maximum A-weighted sound pressure level
L_{eq}	=	equivalent sound pressure level
L_E	=	sound exposure level
M	=	acoustic Mach number
P	=	pressure, Pa
T	=	temperature, K
$\boldsymbol{T}$	=	total thrust, N
V	=	airspeed, ms^{-1}
$\boldsymbol{x}(x_1, x_2, x_3)$	=	Cartesian coordinate system
$\boldsymbol{z}(r, \theta, z)$	=	cylindrical polar coordinate system

*PhD Candidate, ISVR, University of Southampton, AIAA Member
†Professor of Aeroacoustics, ISVR, University of Southampton, AIAA Member.
‡Research Fellow in Experimental Aerodynamics, Applied Aerodynamics Group, Cranfield University, AIAA Member.
§UAV Specialist Technician, Faculty of Engineering and Physical Sciences, University of Southampton
¶UAV Specialist Technician, Faculty of Engineering and Physical Sciences, University of Southampton
‖Senior Enterprise Fellow, Faculty of Engineering and Physical Sciences, University of Southampton
**CASCADE Research Fellow, Faculty of Engineering and Physical Sciences, University of Southampton
††PhD Candidate, Faculty of Engineering and Physical Sciences, University of Southampton

ρ = density, kg m^{-3}

Subscripts

0 = total properties of a thermodynamic variable
amb = ambient properties of a thermodynamic variable
app = relative to approach operation
to = relative to takeoff operation

II. Introduction

The use of Unmanned aerial vehicles (UAVs) for research applications has grown substantially in the last decades. Worldwide research groups have been involved in the design, manufacture, and fly of UAVs. At the University of Southampton, the Soton UAV research team have developed air vehicles for a series of applications, including low-cost reconnaissance and surveillance missions, long range cargo transport missions, underwater robot delivery, fire detection in the Amazon rainforest, and continuous monitoring of volcanic activity.

In addition to research applications, commercial uses of drones as methods of delivering medical supplies to hospitals [1], or package/food delivery services have seen an increase in attention and viability research. Such applications require large volumes of payload to be transported daily. In order to meet such demands, UAV operations will inevitably be high, especially around the centralised distribution hubs. The operation of large fleets of UAVs around these hubs are closely analogous to the operation of commercial transport aircraft. Noise pollution due to proximity to the ground, as well as takeoff and landing high power requirements is severely increased.

The platform named 'Spotter' is one of the most sophisticated and robust fixed-wing UAVs developed by the UAV Soton group [2]. To name just a few activities, the Spotter UAV has been used to investigate maritime incidents and emergencies at sea, to conduct routine operations outside of line of sight, and to investigate environments where rapid response is paramount. The state-of-the-art 35 kg heavy Spotter performed a flight display at Farnborough International Airshow in 2016.

Although the total noise produced by a fixed-wing, small UAV is much lower compared to a light aircraft (e.g., Cessna 172), UAVs low-altitude flight path usually culminate in the air vehicles operating closer to observers on the ground. In surveillance missions, for example, the air vehicle could flyover stationary observers several times during a single flight. The highly tonal noise of these small propeller, piston-engine air vehicles also induce a psychoacoustic problem originating not only from loudness, but also from the annoyance induced by the UAV's unique acoustic signature.

The assessment of the impact of a UAV based delivery network on noise exposure on the ground is a multistep process. Initially a database of noise data for UAVs, adequate to be used in commercial (e.g., AEDT) or academic (e.g., RANE v2) airport noise software must developed. This data must be generated through a combination of measurements and numerical method. The data, as is industry standard, must be in the form of Noise-Power-Distance (NPD) curves. These curves provide the connection between the noise at given observer distance, while an UAV performs a constant altitude and power setting flyover. Previously mentioned airport noise tools may then be used to assess the noise on the ground due to UAV single operation or even fleet operation over the duration of a full day for example. In combination with the capabilities of generating NPDs for propeller power air vehicles [3], and the airport noise tool RANE v2 [4], the global assessment of noise exposure of such UAV networks.

This paper deals with the first step of the process, the generation of reference data. Although reference data for full scale transport aircraft is publicly available through databases such as the Aircraft Noise and Performance (ANP) database [5], NPD data for small scale drones is either scarce or nonexistent. Previously developed frameworks [6], [3] that predict the noise of novel aircraft as functions of changes in aircraft design technology and/or operations require knowledge of baseline noise data for a reference aircraft of similar performance and scale. Overturning the lack of this data is the major contribution of this ongoing research.

UAV flyover measurements are used to develop NPD curves for small scale fixed wing UAVs. The Spotter UAV was used to perform a series of straight and level flyover operations. The SAE-AIR 1845 computational methodology is then used to generate the NPD curves for a number of different power settings. Finally, a simple comparison of the NPD curves to published ones for a light general aviation (GA) aircraft is discussed.

As this research evolves, high-quality acoustic data will be obtained to 1) compute noise contours based on modified

NPD curves for UAVs, 2) develop noise metrics appropriate to this air vehicle category, and 3) provide insight into future noise certification procedures of fixed-wing UAV platforms.

III. Methodology

A. Vehicle and flight data

The Spotter is a light, fixed-wing UAV which uses two four-stroke petrol engines as power plant. Images of the Spotter during ground preparation and during flight are illustrated in Fig. 1.

Fig. 1 Spotter fixed-wing UAV during ground preparation (left) and in flight (right).

The key properties of this vehicle are:

1) 4-meter wingspan
2) cruise speed of 55 knots
3) maximum takeoff weight of 35 kg
4) maximum payload of 5 kg

Flight data is recorded by a digital acquisition system mounted on the vehicle. The barometric pressure, temperature, relative humidity, and wind speed were acquired using a Davis Vantage Pro2 6152 wireless professional weather station mounted in the aerodrome during the experiments. More information about the Spotter can be found in [2, 7].

B. Acoustic Measurements

Two sound level meters (a Svantek SVAN 977, and a B&K Type 2250), and two high-level, high-frequency microphones (B&K 1/4" free-field microphone capsules) were used to measure the noise from three specific manoeuvres, namely, 1) a steady level flyover, 2) takeoff and 3) landing. Multiple flyover operations were performed for the purpose of generating a series of NPD curves and for evaluating the repeatability of outdoor UAV acoustic measuremnts. Measurements at takeoff and approach are performed to extend the current model capabilities and validate noise contour maps in future studies. Both the sound level meters as well as the B&K condenser microphones were placed on tripods 1m off the ground. A schematic is displayed in Fig. 2.

Ambient properties (pressure, temperature, relative humidity, wind speed, and wind direction) were recorded using two Davis Vantage Pro2 Wireless Weather Stations mounted in the air field. Weather conditions were calm to moderate in both tests. All datasets considered in the paper were acquired under average wind speed of 6 m/s and gusts of 10 m/s in a relatively warm day in the UK (12°C), and relative humidity of 75%. Data from the weather station was recorded independently of the acoustic and UAV acquisition systems.

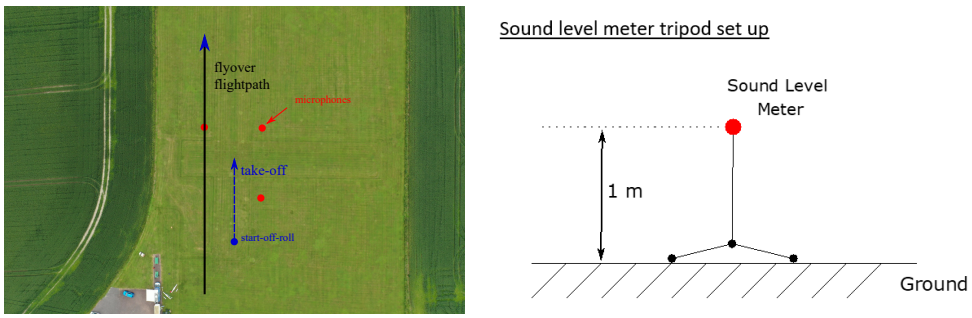

Fig. 2 Diagram depicting the Sound Level Meter locations at Draycot aerodrome (left). Sensor tripod configuration used (right).

1. Test I: steady flyover

Several steady flyovers were performed at 50%, 75% and 100% of available throttle. The distances from the ground varied from 9 m to 27 m. Although only one acoustic sensor under the flight path is enough for this experiment, additional microphones were located on the sideline to investigate lateral effects. These sensors are also used to account for repeatability, uncertainty and errors. Fig. 3 illustrates a schematic of the flyover test.

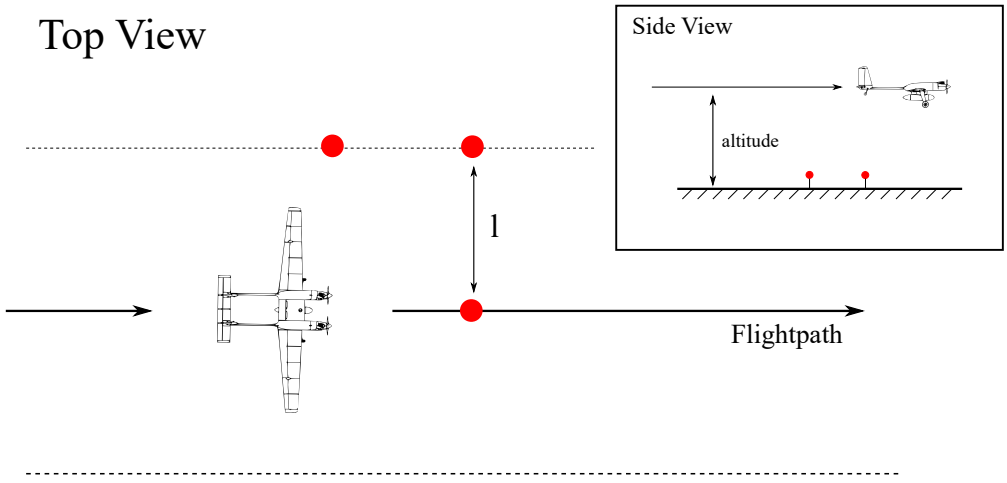

Fig. 3 Schematics illustrating the flyover test procedure.

2. Test II: takeoff and landing

Fig. 4 displays a diagram for takeoff and landing tests. The same flight profile is used for the different payload tests. This is defined by the heaviest configuration tested. Flight data can be used to determine accurately climb and approach angle, airspeed, and rate of climb.

The microphone locations were chosen to replicate the certification points of full scale transport airport under the ICAO Annex 16 [8] as closely as possible. These locations, obtained by moving the microphones during several takeoff and landing tests, may be seen in Fig. 4.

3. Test III: static measurements

Static measurements were performed for five power settings, namely, idle condition, 25%, 50%, 75%, and 100% of available throttle. Sound level data was recorded at azimuthal angles ranging from 0 to 360°, and at 45° intervals.

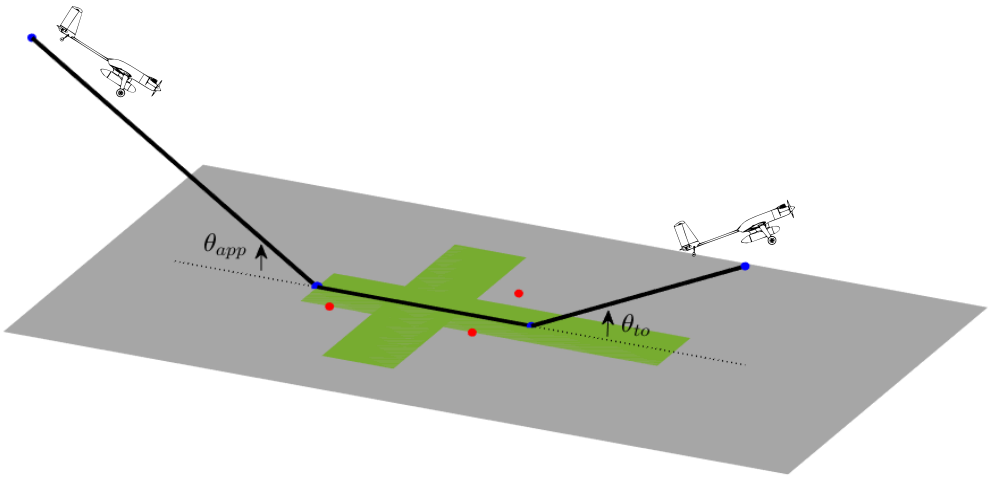

Fig. 4 Schematics illustrating takeoff and landing tests.

C. NPD calculation procedure

This section describes the procedure of processing in-flight experimental data into NPD curves for the future use of assessing noise on the ground due to large number of UAVs operating in various networks.

1. NPD experimental procedure

The NPD development procedure is explained in detail in the SAE AIR document and briefly described below. It is comprised of two principal components, the experimental part and the computational part. The typical flyover procedure setup can be seen in Figure 5. The observer location is positioned directly below the flight track. Doc29 [9] defines slant distance as the shortest distance between any point on the flight track and the observer, or mic location in the experimental case. In the case of constant altitude and speed flyovers the slant distance, d is equal to the flight altitude, h. The flyovers are then performed at different power settings corresponding to settings typically used while performing departure or approach operations. Sound Exposure Levels and $L_{A,max}$ levels and position of occurrence (indicated by polar angle $\theta(j)$ and distance R_p in Figure 5) are then measured giving one point on a NPD curve.

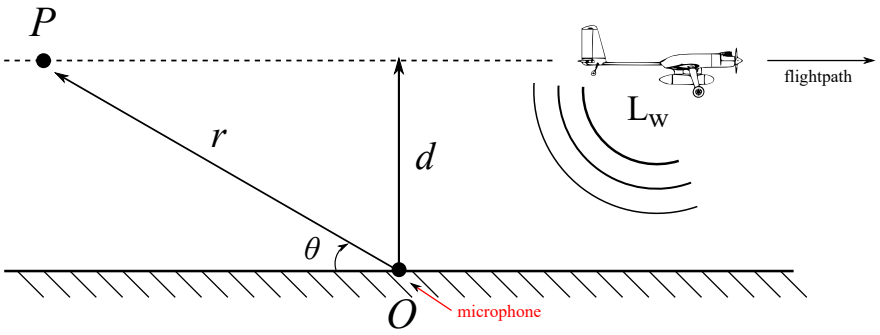

Fig. 5 Diagram of typical flyover procedure for obtaining NPD data. Adapted from [6].

The experiment aims at measuring the $L_{A,max}$ and SEL of the test flyover, for a set of pre-defined engine power settings, yielding the SEL NPD points referred to as baseline levels and marked with a red cross in relevant NPD curve figures. The baseline point is the starting point of the SAE AIR 1854 computational step, alongside spectral information of the flyover.

2. Computation of baseline level from experimental data

Under ideal circumstances, all points on NPD curves would be generated through the experimental component of the procedure alone. However, due limitations on cost, time and measurement opportunity, the number of different operations flown and measured at the expeditions is significantly reduced.

In order to generate a fully experimental NPD data set, all UAV configurations/power settings would perform flyovers over a range of different altitudes. This would provide experimental data for all necessary point on the NPD curves covering all possible combinations of power setting and slant distance used to model takeoff and approach procedures. As this is not possible, single baseline levels levels are used. For each power setting, the flyover is performed at a single altitude. The measurement of this flyover produces a single point on the NPD curve for that power setting. The rest of the points are generated computationally by the procedure described in the following section. Figure 6 depicts an example set of SEL NPD curves for a de Havilland Canada DHC-6 Twin Otter in a takeoff configuration. The red crosses depict the baseline points that are measured, while the rest of the points are computed. Two power settings are shown, 30% and 100% of maximum static thrust.

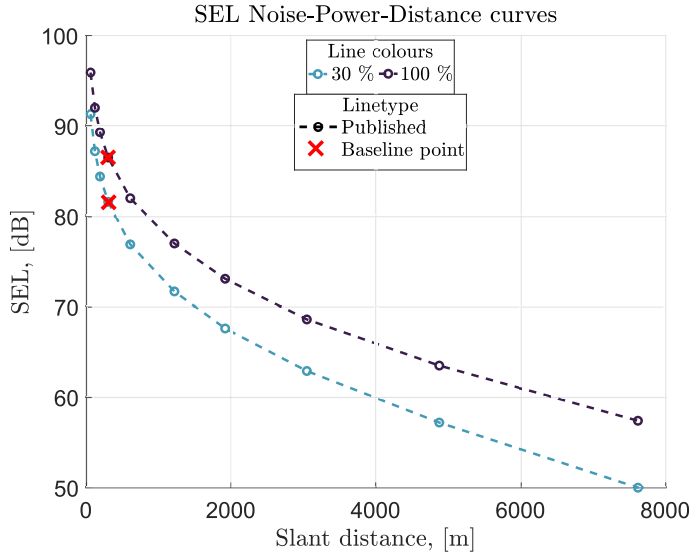

Fig. 6 Example of a takeoff SEL NPD for the DHC-6 Twin Otter, indicating the baseline levels. Data is from the ANP database [5]

The metrics of interest are in $L_{A,max}$ and SEL. The sound level meters records the instantaneous A-weighted sound level L_A every 10 ms as well as the one-third octave band frequency spectra. By definition, $L_{A,max}$ is simply the maximum level that occurs during a flyover in the L_A time history.

The sound exposure SEL or otherwise L_{AE}, with the subscript "A" also denoting the metric is A-weighted, is not a direct output of the sound level meter. The SEL may be calculated directly by its definition as the one second long steady level containing equivalent total acoustic energy as the actual fluctuating noise,

$$L_{AE} = 10 \log \left(\sum_{i=1}^{n} 10^{L_{A,i}/10} \Delta t \right) \tag{1}$$

3. SAE AIR 1845 computational step and construction of NPD curves

The steps in producing NPD curves for propeller powered UAVs from a baseline measured NPD point are almost identical to that of conventional aircraft. For detailed explanation the reader is encouraged to follow the procedure described in [6] and [9] along with the SAE AIR1845 [10] computational step.

The procedure is outlined in a number of bullet points where differences between propeller UAVs and conventional turbofan aircraft are specified.

- Baseline levels and one-third octave band spectra at each power setting are acquired through experimentally measured $L_{A,max}$ NPD level at distance d (or equivalently altitude h) and polar angle θ.

- Spherical spreading adjustment is performed for every slant distance of interest. This is done for every power setting.
- Using the one-third octave band spectrum, atmospheric attenuation adjustment is performed. This adjustment takes into account the propagation distance as a function of the slant distance and the polar angle at which the maximum level occurs θ_{max}. The attenuation rates used are defined by the SAE AIR-1845 atmosphere and are a function of frequency as well as distance.
- For each power setting, all NPD distance d_i the spectra are A-weighted and decibel-summed to determine the resulting A-weighted levels $L_{A,max}$.

At this point $L_{A,max}$ NPDs have been derived. The next few steps summarise the procedure for the development of SEL or L_{AE} NPDs

- Using the instantaneous SPL measurements, numerical integration is performed to estimate the SEL / L_{AE} at the microphone locations. This procedure is performed for each power setting at its respective altitude.
- Using the SEL L_{AE} and the previously derived $L_{A,max}$ NPD the SEL L_{AE} is calculated at the remaining NPD slant distances. The exact relation may be found in SAE AIR 1845 [10].
- This procedure is carried out for every power setting of interest.

IV. Results I: Acoustic Measurements

Results and discussions are presented in two main sections. Firstly, in this section, in-flight and static experimental data are analysed. Performance data collected from the UAV as well as acoustic data from flight and static tests are presented separately. Then, in Section V, experimentally computed and modelled NPDs are provided.

A. UAV flight data

The data presented to produce the NPD curves within this study was recorded on the 24^{th} of June 2021. A single UAV mission was used for all in-flight acoustic measurements. This mission was comprised of non-acoustic related measurements and testing for the initial 2/3 of the mission, while the final third was reserved for low altitude flyovers directly above the microphone / sound level meter locations. The ground speed and throttle setting for the entirety of the mission are shown in Figures 7 and 8.

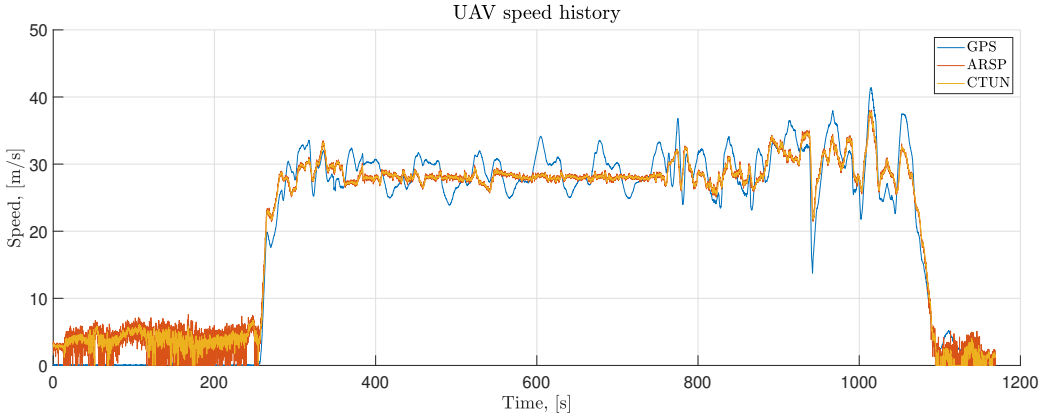

Fig. 7 Spotter ground speed throughout single mission.

The low altitude flyovers occur between $t = 800s$ and approximately $t = 1050s$, with a landing operating taking place shortly after. Five flyover operations take place between those time stamps, with the throttle setting in each one reaching the maximum value of 100%. Ground speed was not maintained constant, with significant fluctuations occurring around the 30 m/s mark. Peak values for each of the flyovers may be seen in Table 1.

B. Flight measurements (preliminary results)

Before and after each flight, the background noise was measured for 60 seconds. As expected, a relatively large variation is seen in the background sound pressure spectrum. An example is illustrated in Fig. 9. The sound pressure

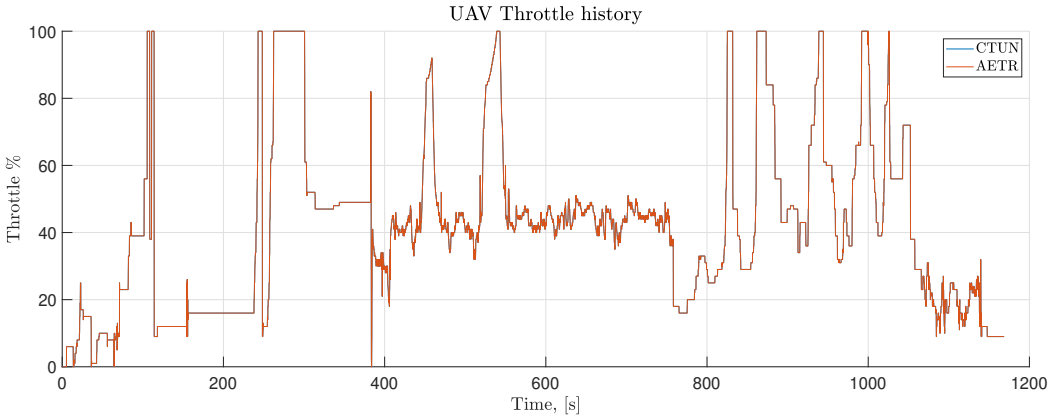

Fig. 8 Spotter throttle setting throughout single mission.

Table 1 Maximum speed during flyover operations.

Flyovers	**1**	**2**	**3**	**4**	**5**
Max speed , [m/s]	31.2	34.1	34	38	33

level was obtained for every one second for the background data before and after a flight test (120 curves in total). These data was obtained in the first experiment, in which the weather conditions were poorer compared to the second experiment.

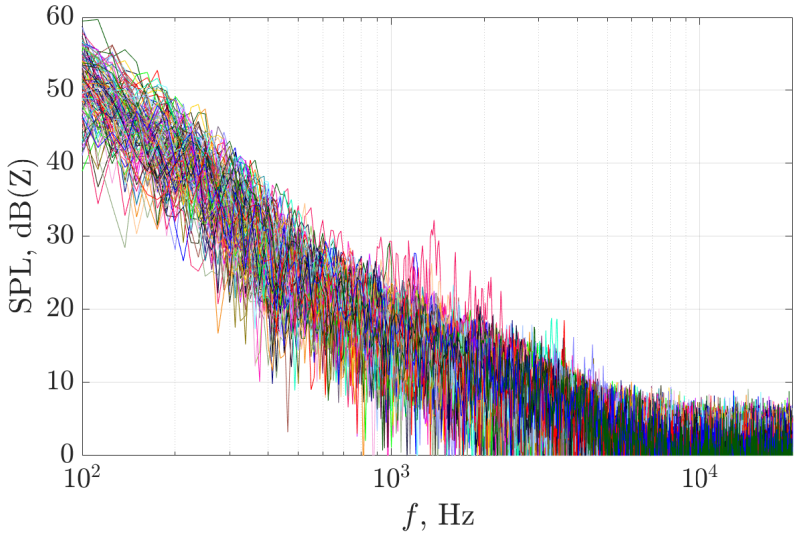

Fig. 9 Background spectra measured before the takeoff and flyover tests reported in figures 10 and 11

Except for very low frequencies, takeoff and flyover recordings produced noise levels at least 6 db higher than the background noise. Therefore, the background noise level used as a reference was simply averaged from the data and no corrections based on the weather conditions were attempted. Sample results for the SPL measured during the flyover and takeoff tests are displayed in Fig. 10(a) and Fig. 10(b), respectively. For reference, one of the flyover spectrum is also shown in Fig. 10(b). The averaged background noise is also illustrated. As expected, experimental data for flyover and takeoff test is a statistically non-stationary process. Even when corrections for the distance between the microphones and the Spotter were applied, gusts and wind modify the strength of the low-frequency tones measured

over time. Nonetheless, the Spotter SPL spectra was clearly seen above the background noise and the data can serve as input to producing the NPDs and noise contour maps.

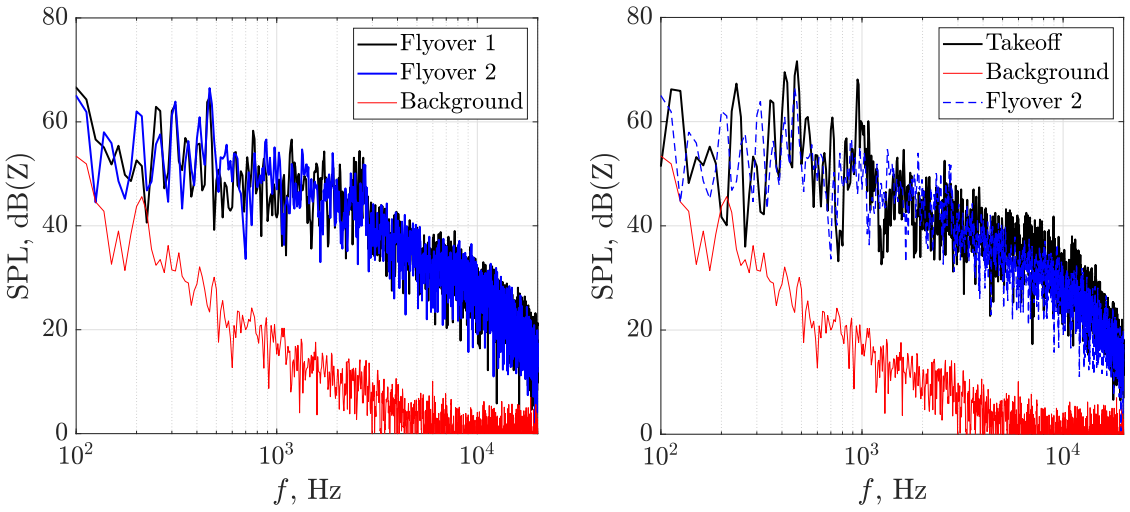

(a) flyover (b) takeoff

Fig. 10 SPL spectra for flyover and takeoff measurements

Finally, a series of SPL spectra (in 0.1 second steps) is shown below, in Fig. 11. The estimated time for the shortest distance between the air vehicle and microphone used is indicated by a black, dashed line. Both the internal clock of the flight data and acoustic acquisition systems were synchronised with 0.5 s precision. Part of the future work also involves automatising the communication between all control and acquisition systems used in the experiment. This is paramount to reducing the uncertainty of the outdoor experiments described here.

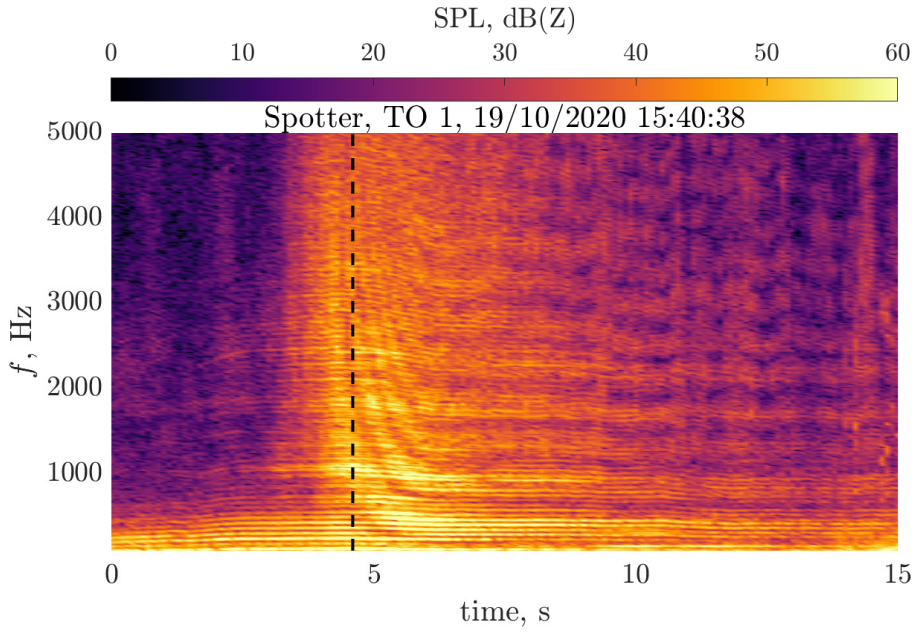

Fig. 11 SPL measured during one of the Spotter's takeoff test

The B&K and Svantek sound level meters directly record averaged values and provide the options of applying A or C frequency weightings. The SPL time histories are given in L_{eq}, which by definition are equivalent continuous

sound levels, time-averaged sound level for the elapsed measurement time. For the B&K the elapsed time between L_{eq} measurements is 1s, whilst for the Svantek its 0.7s. The basis of all calculations that proceed are the $L_{A,eq}$ time histories of the flyover operations. Figure 12 shows the A-weighted L_{eq} as function of time during the entire mission of interest. The altitude during the mission is also plotted for reference. The period of interest occurs in the final third of the mission, where the five (5) large peaks in $L_{A,eq}$ indicate the $L_{A,max}$ of each individual flyover. It is interesting to note the take-off and landing operations that occur at around $t = 80s$ and $t = 900s$ respectively.

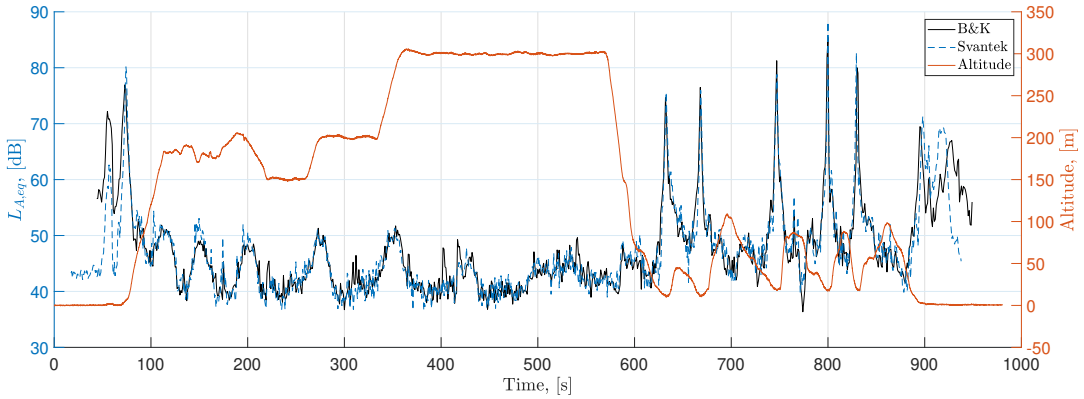

Fig. 12 $L_{A,eq}$ **time history as measured by the B&K and Svantek sound level meters throughout the whole mission. Barometric altitude is also shown on the right hand side y-axis over the same time period.**

The altitude time history provide the slant distance for each of the flyovers, which are summarised in Table 2.

Table 2 Slant distance during flyover operations.

Flyovers	**1**	**2**	**3**	**4**	**5**
Slant distance , [m]	12	12	20	20	20

Figure 13 compiles and compares all flyovers times histories as measured by the B&K sound level meter. The x-axis $t = 0$ denotes the time of $L_{A,max}$ occurrence.

For each of the flyovers, a 10 dB down period relative to $L_{A,max}$ was defined for the calculation of the sound exposure level L_{AE}. In each case integration over the said period using the discrete from of the SEL definition in Equation 1 was performed. A summary of the single event sound levels may be seen in Table 3.

Table 3 Maximum A-weighted SPL and SEL characterising the single event flyover.

Flyovers	**1**	**2**	**3**	**4**	**5**
$L_{A,max}$	74.64	76.48	81.25	85.43	80
L_{AE}	77.7	78.34	82.6	87.1	82.8

In addition to OASPL metrics, the frequency content of the noise signal measured by the sound level meters was also captured. The frequency data, depending on the individual capturing device, is presented in two different forms: in the case of the Svantek, the FFT option was chosen. The frequency range/band was set to 20kHz, while a Z-weighting was applied as per IEC 61672-1:2013 [11]. This results in a narrow-band spectrum of bandwidth equal to 12.5 Hz being captured every 100ms. A sample spectrum may be seen in Figure 14 for Flyover 4 at the time of $L_{A,max}$ occurrence.

In the case of the B&K sound level meter, the frequency content of the noise signal is given in terms of $1/3^{rd}$ octave bands. A total of 32 bands were used with centre frequencies ranging from 12.5 Hz to 16 kHz. A larger integration period is used relative to the Svantek, with spectra being given every 1s. The $1/3^{rd}$ octave bands of each one of five flyover at the point of L_max occurrence is given Figure 15.

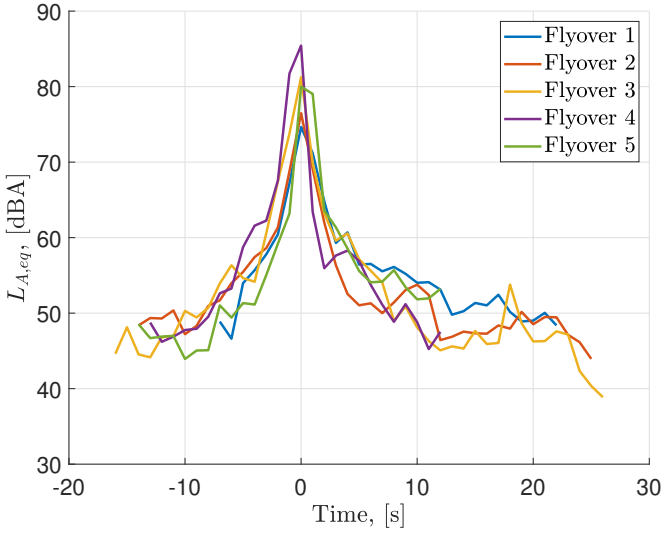

Fig. 13 $L_{A,eq}$ **time history as measured by the B&K sound level meter for the 5 flyovers. Time** $t = 0$ **indicates the occurrence of** $L_{A,max}$ **of each individual flyover.**

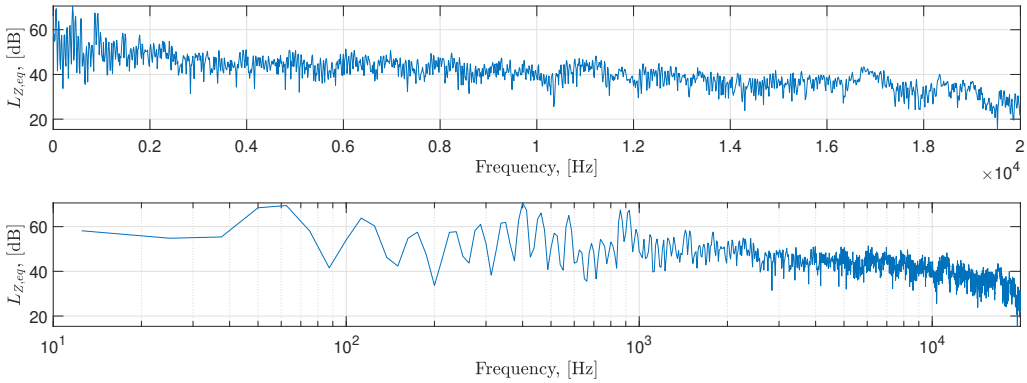

Fig. 14

C. Static measurements

Static measurement results are presented here. The purpose of the static measurements was twofold: (i) a characterisation of the UAV static directivity with the intent of developing empirical directivity functions for future noise exposure contour studies. (ii) quantify the effects of atmospheric conditions on the measurements.

Noise was measured at 8 azimuthal locations around the static UAV. Recording of approximately 10s seconds were used to measure cumulative levels L_{eq} and SEL. The procedure was carried out for both sound level meters, for 5 different throttle settings: 20%, 40%, 60%, 80% and 100%.

V. Results II: Estimating Noise-Power-Distance Curves

Noise-Power-Distance are the main source of input data for airport noise models. In this section, the steady level flyover measurements (typical experimental procedure for full-scale vehicles) of Spotter are used to define the starting point of the $L_{\mathrm{A,max}}$ and SEL metric NPD curves. Then, using an industry standard computational procedure, the noise metrics are evaluated at the rest of the NPD slant distances. The propagation technique accounts for atmospheric attenuation through the use of one-third octave bands derived from the measured narrowband data.

Five flyover operations were studied, as seen in Figure 13. Due to the scale of the UAV, the flyovers were performed

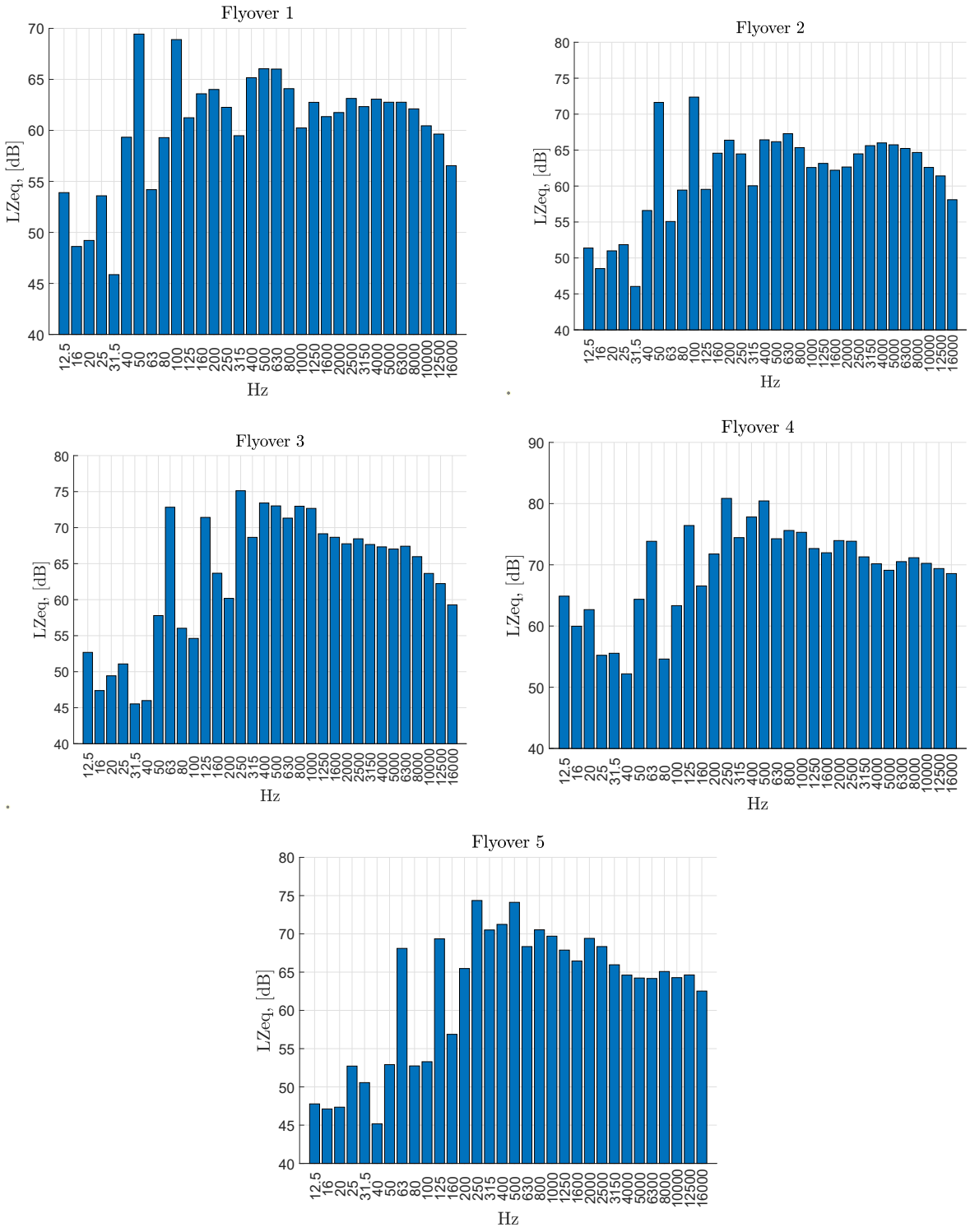

Fig. 15 Unweighted $1/3^{rd}$ Octave band spectra for each of the flyovers. The indicated spectra occurred at the time of $L_{A,max}$.

at a much lower altitude than for conventional fixed-wing aircraft. The standard altitude for NPD measurements is defined in Doc29 [9] as being 1000ft or 305m, in this study the altitudes were reduced by an order of magnitude to that of

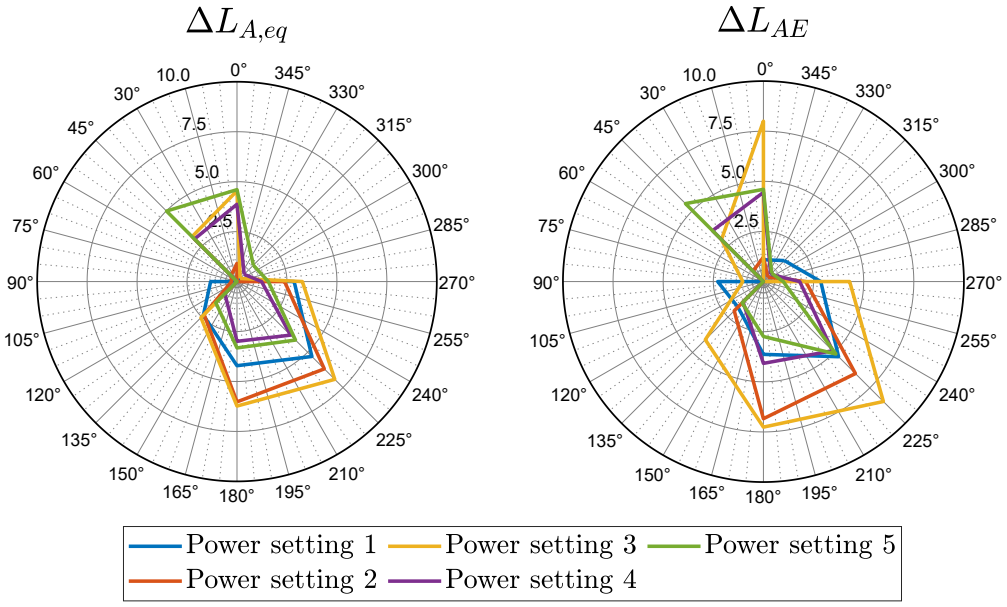

(a) B&K 2550

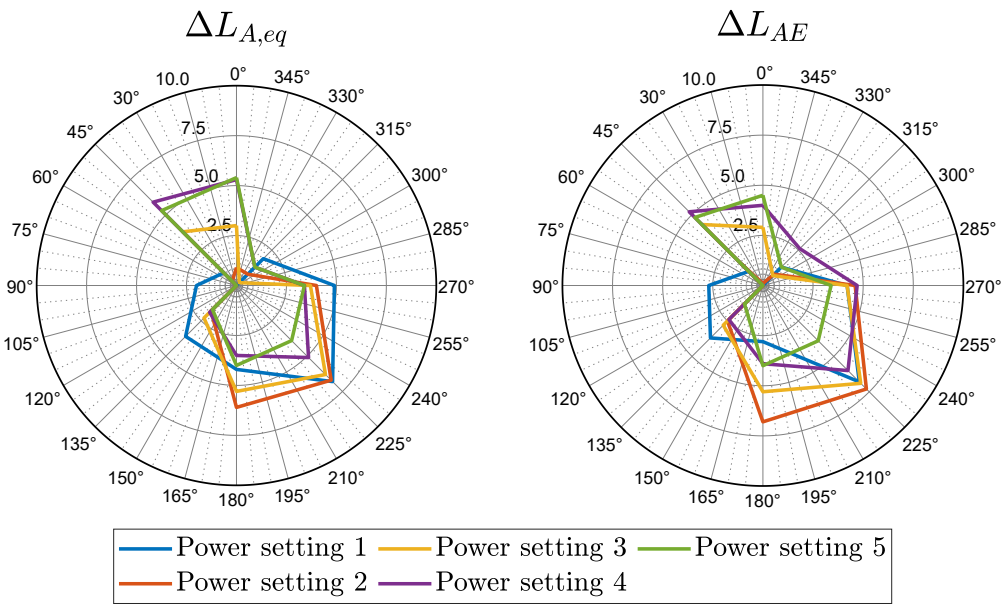

(b) Svantek SVAN 977

Fig. 16 Static cumulative directivity of Spotter UAV. Radial value represents the Δ relative to the minimum value.

approximately 20 m. For exposure level such as the SEL NPD curves, a a time duration correction [9], was applied with a reference speed chosen at 35 m/s. Corrections to atmospheric conditions such as temperature and relative humidity were neglected as no variation in the measured conditions were observed during the period the flyovers were performed.

A. Spotter NPD curves

Due to the altitude of the flyovers being significantly reduced, the NPD curves for the Spotter UAV were calculated for 5 additional slant distances on top of the standard 10 recommended. These additional distance were: 5ft, 10ft, 20ft 50ft, 100ft. The values of Table 3 served as the baseline points and can be seen in Figures 17 marked as black crosses.

Using the un-weighted $1/3^{rd}$ octave band frequency spectra of Figure 15 as representative for each flyover, the standard SAE-AIR 1845 computational procedure was used to generate the $L_{A,max}$ and SEL NPD curves for the Spotter UAV.

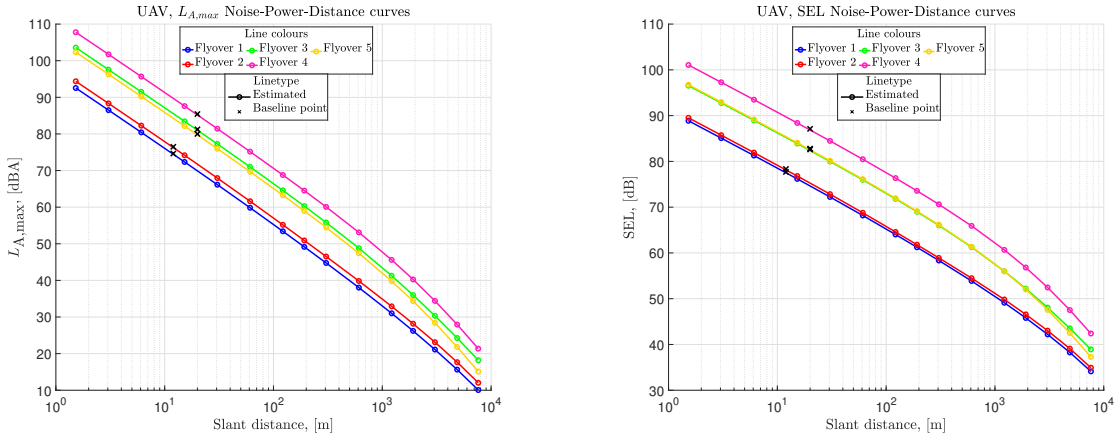

(a) $L_{A,max}$ (b) SEL

Fig. 17 Flyover Noise-Power-Distance curves.

B. Comparison to light aircraft

The Cessna 172 Skyhawk was chosen as a reference comparison aircraft, in order to put the UAV NPD curves into perspective. The Cessna 172 is a single reciprocating engine aircraft with a MTOW of 1111.301 kg (data from ANP database [5]). In comparison the Spotter UAV is a twin reciprocating engine aircraft with a MTOW of 35 kg. The comparison between the NPD curves can be seen in 18.

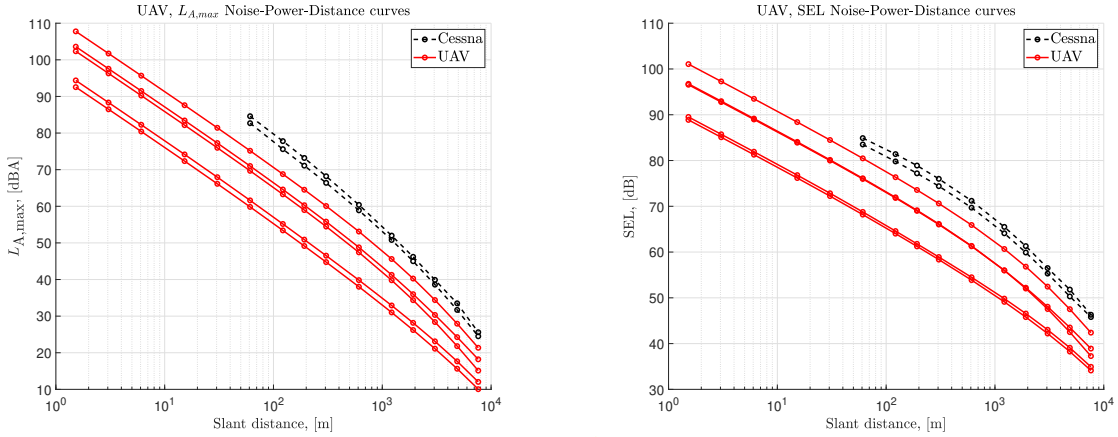

(a) $L_{A,max}$ (b) SEL

Fig. 18 Comparison to Cessna 172 departure NPD curves. All 5 of the flyover are shown for the Spotter UAV, while two power settings for the Cessna, one being 100% of maximum static thrust (MST) and the other 70%.

As expected, the Cessna is louder than the UAV at slant distances. At 61 m, the smallest available slant distance for the Cessna the difference in terms of $L_{A,max}$ is -22.87 and -24.77 dB(A), for the least noisy flyover (flyover 1) and the two Cessna power settings and -7.54 and -9.43 dB(A) for noisiest flyover (flyover 4) respectively.

VI. Results III: Estimating Noise Contours

As mentioned, noise exposure contours are typically generated using high-fidelity airport noise models specifically developed for full-scale aircraft and operations around airports. In this paper, the in-house airport noise model RANE (Rapid Aviation Noise Evaluator)[4, 12] is used. Using the previously derived NPD curves single event noise exposure contours are generated.

Using the UAV data for altitude, speed and position, a simplified two segment flightpath was generated. The two segments comprised of a take-off field run approximated at 50 m and second segment of length equal to 660 m representing the climb to cruise altitude. The inclination angle used for the climb segment was 15.8°. The 75 dB SEL contour was chosen as a realistic and relatively high level that could be observed at the field, despite the unpredictable weather conditions. Lower level contours could be generated using the NPD curves, however if wind speeds and directions are not accounted for, the contours will be highly over-predicted. Figure 19 shows the 75 dB SEL contours as generated using the NPD from each flyover.

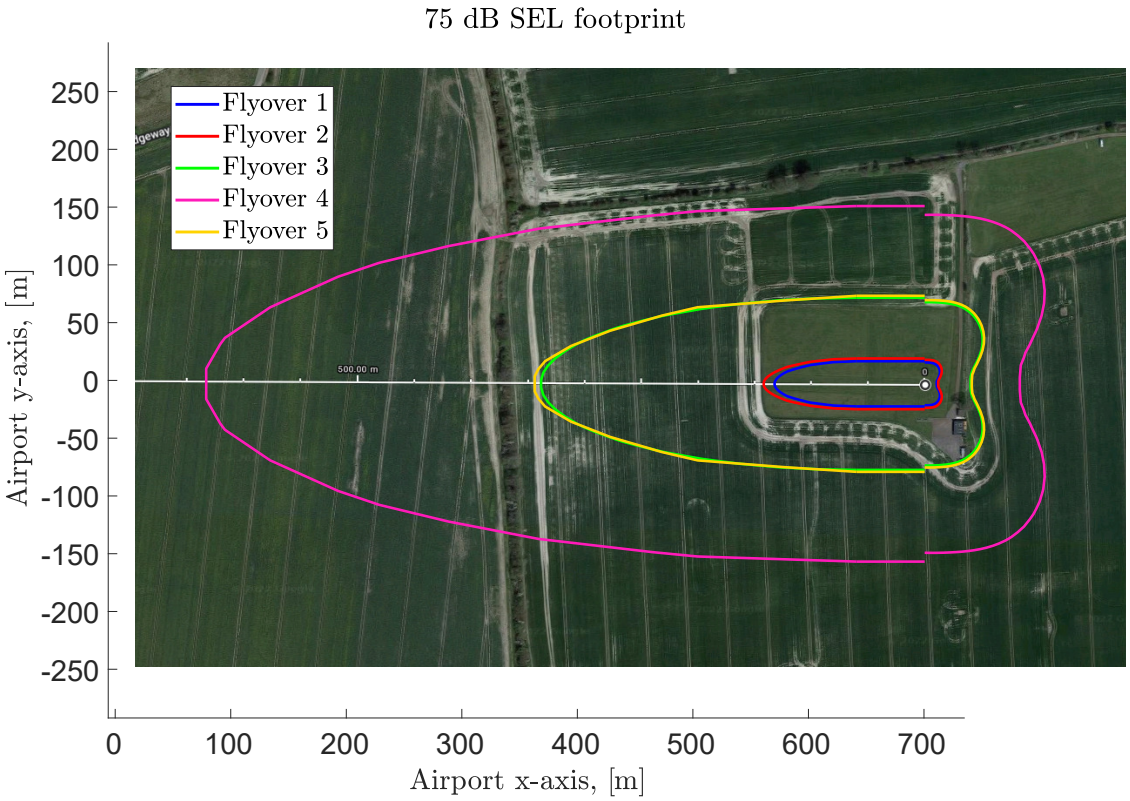

Fig. 19 75 dB SEL contours generated using airport noise tool RANE for each of the flyover NPDs. The contours are shown in the context of Draycot aerodrome where the measurements took place.

The power setting is assumed to be constant throughout each segment and no variation in power occurs from the ground roll to climb. The power setting for each flyover is representative of the PWL the aircraft is radiating if it were to be regarded as a lumped source.

VII. Conclusion

Preliminary outdoor noise measurements for a fixed-wing UAV have been described. The data was acquired at two separate expeditions, one smaller and one larger. Both static and in-flight conditions were of interest; the first for characterising the directivity of the dual propeller setup, while the second for the purpose of generating NPD curves and the assessment of noise on the ground due to take-off and landing operation of UAVs.

The Spotter, a 35 kg light UAV, is currently used in a broad range of research activities. The CAA and industrial partners have required detailed information about the noise footprint of this platform, which is one of the main motivations for the current work. Additionally, formal noise certification procedures are yet to be developed for similar

versatile air vehicles. The noise measurements carried out in this work were based on acoustic experiments performed for manned fixed-wing aircraft. Thus, this unique experimental dataset underscores both the requirement to synchronize flight telemetry with ground data, and the necessity to develop noise certification procedures for small vehicles flying outdoors.

A total of five flyovers were used to assess the noise of a fixed wing UAV. The flyovers were flown at full throttle, while trying to maintain constant altitude and speed. Each flyover is characterised by an $L_{A,amx}$ level and an SEL. These levels were then used to generate 5 distinct NPD curves. When corrected for variation in exposure time and altitude the difference between the lowest and highest predicted $L_{A,amx}$ NPD at a slant distance of 100 m was approximately 15 dB(A), whereas for the SEL NPD 11.5 dB. This exceeds the average error range (± 1.5 dB for the $L_{\mathrm{A,max}}$ NPD curves and ± 2 dB for the SEL NPD curves) suggested by ECAC Doc29 and ANP database for full scale conventional aircraft. This indicates to a few possible differences that arise between the flyover measurements: (i) difference in background noise levels (ii) additional noise sources contributing to the overall PWL and (iii) variation in the PWL of the matching source mechanisms.

A brief list of observations and conclusions is presented below:

- Small scale outdoor measurements prove difficult due to weather conditions. Background noise is in many cases comparable to the relatively lower PWL of the UAV noise sources.
- large error in UAV NPD curves as a result of large variation in L_{max} between flyovers. This results in large error in contour location and area.
- UAV performance is variable. Flyovers need to be closer to steady-level conditions.
- propeller RPM data could help identify contribution of individual sources and help identify the possibility of unexpected noise sources dominating.

As with passenger aircraft, future regulations and policies may require UAVs to remains bellow specific limits. Potential large scale employment of cargo drones, may see the development of UAV traffic routes above urban residential areas, however, bellow any flight level that may cause interference with large scale aircraft traffic movement. Methods of establishing these limits are yet to be developed, and the noise emitted by small scale it yet to be fully understood. Techniques used for full scale aircraft may prove ineffective at capturing the realistic noise exposure due to UAVs. Expeditions such as the ones presented provide the stepping stones for developing appropriate methodologies to be applied to UAVs.

References

[1] "Solent NHS drone trials," , 2022. URL `https://apian.aero/solent.html`, accessed on 13/01/2022.

[2] Ferraro, M., Lock, A., Scanlan, J. P., and Keane, A. J., "Design and flight test of a civil unmanned aerial vehicle for maritime patrol: the use of 3D-printed structural components," , 2014. URL `https://eprints.soton.ac.uk/37420/`.

[3] Amargianitakis, D., Self, R., Torija, A., Proenca, A., and Synodinos, A., "Towards predicting Noise-Power-Distance curves for propeller and rotor powered aircraft," *Internoise Proceedings*, 2021.

[4] Amargianitakis, D. C., Self, R. H., Torija, A. J., Proenca, A., and Synodinos, A. P., "Closed-form analytical approach for calculating noise contours of directive aircraft noise sources," *AIAA AVIATION 2021 FORUM*, 2021. https://doi.org/10.2514/6.2021-2175, URL https://arc.aiaa.org/doi/abs/10.2514/6.2021-2175.

[5] Centre, E. E., "Aircraft noise and performance (ANP) database v2.1," , 2016. URL http://www.aircraftnoisemodel.org.

[6] Synodinos, A. P., Self, R. H., and Torija, A. J., "A framework for predicting Noise-Power-Distance curves for novel aircraft designs," *Journal of Aircraft*, 2017.

[7] Soton UAV, "Spotter facts and figures," , May 2021. URL https://www.sotonuav.uk/platforms/spotter/.

[8] ICAO, "Annex 16 to the Convention on International Civil Aviation: Environmental Protection, Volume I Aircraft Noise," Tech. rep., International Civil Aviation Organization, July 2017.

[9] "Report on standard method of computing noise contours around civil airports, vol. 2: Technical guide," Tech. rep. ecac.ceac doc. 29, 4th ed, European Civil Aviation Conference (ECAC), December 2005.

[10] "Society of Automotive Engineers: Procedure for the Calculation of Aircraft Noise in the Vicinity of Airports," Tech. Rep. 1845, SAE AIR, 1981.

[11] "En 61672-1:2013 - electroacoustics - sound level meters - part 1: Specifications," , ???? URL https://standards.iteh.ai/.

[12] Torija, A. J., Self, R. H., and Flindell, I. H., "A model for the rapid assessment of the impact of aviation noise near airports," *The Journal of the Acoustical Society of America*, , No. 2, 2017, pp. 981–995.